Microultrasound characterisation of *ex vivo* porcine tissue for ultrasound capsule endoscopy

IOP Conf. Series: Journal of Physics: Conf. Series **797** (2017) 012003 doi:10.1088/1742-6596/797/1/012003

Microultrasound characterisation of *ex vivo* porcine tissue for ultrasound capsule endoscopy

H S Lay[1], B F Cox[2], M Sunoqrot[2], C E M Démoré[3], I Näthke[2], T Gomez[4], S Cochran[1]

[1]University of Glasgow, Glasgow, UK
[2]University of Dundee, Dundee, UK
[3]Medical Biophysics, University of Toronto, Toronto, Canada
[4]Spanish National Research Council, Madrid, Spain
holly.lay@glasgow.ac.uk

Abstract Gastrointestinal (GI) disease development and progression is often characterised by cellular and tissue architectural changes within the mucosa and sub-mucosa layers. Current clinical capsule endoscopy and other approaches are heavily reliant on optical techniques which cannot detect disease progression below the surface layer of the tissue. To enhance the ability of clinicians to detect cellular changes earlier and more confidently, both quantitative and qualitative microultrasound (μUS) techniques are investigated in healthy *ex vivo* porcine GI tissue. This work is based on the use of single-element, focussed μUS transducers made with micromoulded piezocomposite operating at around 48 MHz.

To explore the possibility that μUS can detect Crohn's disease and other inflammatory bowel diseases, *ex vivo* porcine small bowel tissue samples were cannulised and perfused with phosphate-buffered saline followed by various dilutions of polystyrene microspheres. Comparison with fluorescent imaging showed that the microspheres had infiltrated the microvasculature of the samples and that μUS was able to successfully detect this as a mimic of inflammation. Samples without microspheres were analysed using quantitative ultrasound to assess mechanical properties. Attenuation coefficients of 1.78 ± 0.66 dB/mm and 1.92 ± 0.77 dB/mm were obtained from reference samples which were surgically separated from the muscle layer. Six intact samples were segmented using a software algorithm and the acoustic impedance, Z, for varying tissue thicknesses, and backscattering coefficient, BSC, were calculated using the reference attenuation values and tabulated.

1. Introduction

Ultrasound endoscopy represents the state-of-the-art in clinical diagnostic tools for diseases of the human gastrointestinal (GI) tract. High-definition optical imaging is used in conjunction with ultrasonic imaging to visualise the surface and penetrate the thickness of the tissue to identify the cellular and tissue architectural changes induced by disease. This technology is limited, however, by the length of the endoscope probe, rendering the full extent of the GI tract difficult to visualize properly.

Video capsule endoscopy (VCE) is a technology which is just now reaching maturity after two decades of development, using physical implementation as a capsule to eliminate the probe length limitations of standard endoscopes and allowing visual diagnosis of the full length of the GI tract [1]. However, current capsules can perform only optical imaging, limiting their diagnostic capability. This has motivated research into expanding the diagnostic modalities available in capsule format [2],

including research seeking to develop ultrasound capsule endoscopy (USCE) integrating microultrasound (μUS) imaging systems with high-quality optics and additional modalities.

Coeliac disease and inflammatory bowel disease (IBD) such as Crohn's disease represent common clinically encountered gastrointestinal disorders that significantly affect the health and well-being of patients. VCE has been indicated in the management of both conditions because of its ease of use and acceptability to patients as compared to standard endoscopy [3]. However, the lack of subsurface imaging available in VCE limits its usefulness in the diagnosis of early Coeliac or Crohn's disease, as both disorders originate below the surface of the mucosa [4]. For this reason, the functionality of μUS imaging, above the standard range of 1-20 MHz, merits investigation in examining the layer structure of healthy GI tissue and modelling subsurface inflammation similar to that seen in Crohn's and Coeliac disease.

It has already been shown that μUS can be used to characterize GI tissue with a high level of agreement with histology [5]. This paper first reports qualitative studies of healthy tissue and tissue treated with microspheres to mimic inflammation. In addition to qualitative analysis, μUS can also be used to determine the mechanical properties of tissue based on its effects on acoustic wave propagation and related investigations have shown that quantitative μUS can be used to detect pre-cancerous changes in tissue structures [6]–[9]. Two measures which have been identified as of interest to this study are the acoustic impedance (Z) and backscattering coefficient (BSC), which have shown potential for detecting cellular and tissue architectural changes characteristic of early disease stages [6].

A disease whose progression includes the types of cellular change that may be addressed is Barrett's Esophagus (BE). In BE, the distal squamous mucosal layer of the esophagus undergoes a metaplastic transformation and is replaced by a simple columnar layer. BE affects approximately 2% of the UK population [10] and is considered a pre-malignant condition at risk of developing into oesophageal cancer. For this reason, oesophageal tissue samples were targeted for quantitative analysis, focusing on measurements of the type that could be performed *in vivo* to allow Z and BSC to be calculated.

In this paper, *ex vivo* porcine tissues were used in both the qualitative and the quantitative studies to establish a healthy baseline and to establish resolution thresholds in the measurements proposed. Emphasis was placed on measurement techniques which could be translated to *in vivo* clinical implementation with USCE with a minimum of change, so calibration scans are used for those measurements which could not be performed without a ground truth reference.

Healthy swine oesophageal and small bowel tissue was chosen primarily because the histology of the porcine gastrointestinal tract resembles that of humans at the squamocolumnar junction [11]. As tissues were obtained fresh-frozen from the abattoir post-mortem, ethical approval was not necessary. While the frozen state of the tissue was a consideration, freeze-thaw cycles have been shown not to affect the acoustic properties of tissue, allowing them to be used in the analysis without concern [12].

2. Tissue Characterisation

2.1. Qualitative Imaging

The feasibility of an ultrasound-based endoscopic capsule system will be dependent on the ability to distinguish health-related changes in the subsurface structure of the GI tract. To investigate this, we generated single-element microultrasound transducer scans of healthy porcine GI tissue and examined them qualitatively to establish base-line values against which diseased tissue could be assessed. To mimic the tissue inflammation seen in Crohn's disease and Celiac disease, fluorescent microspheres were infused into cannulised bowel tissue and imaged both optically and with μUS. The fluorescent properties of the microspheres allowed them to be visualised optically while their acoustic properties were assessed in the μUS images.

2.2. Quantitative Measures

2.2.1. Attenuation

As the tissue samples analysed for this paper were of non-negligible thickness, it was critical to assess and compensate for the loss-factors which could skew the raw echo data and bias the resulting values. Some of these factors cannot be measured in *in vivo* tissue because of a lack of ground truth references, so typical values are calculated from *ex vivo* tissue samples with similar properties using the same scanning set up. By placing the *ex vivo* tissues on top of a highly-reflective substrate and imaging the substrate both with and without the intervening tissue, the two-way attenuation of the tissue can be measured. While attenuation in the tissue is caused by both absorption and scattering, which are frequency dependent, a bulk attenuation factor can be calculated which will be consistent for tissue of a specific type and similar thickness scanned with the same centre frequency.

For a tissue sample with known thickness d, the attenuation factor (α) in dB mm^{-1} can be calculated as:

$$\alpha = \frac{-20}{2*d}\log_{10}\frac{V_r}{V_a}, \tag{1}$$

where V_r is the amplitude of the reflected signal received from the reference reflector beneath the tissue and V_a is the amplitude of the signal reflected from the reference reflector with no masking tissue. The logarithmic attenuation coefficient (dB mm^{-1}) can then be converted to the natural logarithmic a' (neper mm^{-1}) via:

$$a' = \frac{\alpha}{8.686}. \tag{2}$$

2.2.2. Acoustic Impedance

The characteristic acoustic impedance of a tissue, Z, is a function of the density and wave velocity of a tissue, and thus can be used to determine if changes in the overall density have occurred because of re-organization of the cellular structure or changes in the fluid levels. If the tissue of interest is embedded in a fluid of known impedance, the easiest method to calculate the impedance is through analysis of the echo reflection as a function of the reflection from a known material. For both the known and unknown materials, the reflected wave amplitude (V_r) is a function of the incident wave amplitude (V_i) and the acoustic impedances of the two media,

$$V_r = \frac{Z_t - Z_w}{Z_t + Z_w}V_i, \tag{3}$$

where Z_t is the acoustic impedance of the material under investigation and Z_w is the acoustic impedance of the imaging medium, given a perpendicular incident wave and $Z_t > Z_w$. Rearranging for the unknown target acoustic impedance results in a solution for Z_t (MRayl):

$$Z_t = -\frac{V_r + V_i}{V_r - V_i}Z_w. \tag{4}$$

The known reflector is used to solve for V_i using the inverted version of eqn 3:

$$V_i = \frac{1}{R_q}V_r, \tag{5}$$

where R_q is the reflection coefficient defined by:

$$R_q = \frac{Z_t - Z_w}{Z_t + Z_w}. \quad (6)$$

Solving this equation for the reference reflector (a quartz flat with known material properties) results in a value for V_i, which can then substituted into Eqn. 4 to solve for Z_t for the unknown material.

2.2.3. Backscatter Coefficient

Calculating the BSC of a material can provide insight into the distribution and properties of scatterers which are smaller than the imaging wavelength. These would be otherwise invisible to normal ultrasound imaging. Because of the dependence of backscatter on the scanning procedure and transducer properties, the calculations in this paper are based on the technique derived by Foster et al [13] for use with single-element focused transducers. Using this derivation, E_S, the energy received by the transducer after scattering by the tissue can be written as:

$$E_s = KI_0A \int_S \mu(\theta)\, d\Omega \int_{d_1}^{d_2} e^{-4a'l} dl, \quad (7)$$

where K is a constant propagation factor, I_0 is the incident acoustic intensity from the transducer, and A is the surface area of the transducer face. The differential scattering coefficient, $\mu(\theta)$, is integrated over the surface of the receiver, S, and the attenuation coefficient, a', is integrated from d_1, the minimum depth of the tissue window, to d_2, the maximum depth of the tissue window [13].

Breaking up Eqn. 7 to isolate terms, it can be shown that the first term is dependent on the scanning transducer characteristics and the last term is a function of the attenuation properties of the material. Using a known ground truth reference similar to that used in the acoustic impedance measurements, the first term can be cancelled out by obtaining a reference scan with the same scanning setup as the tissue scans. By substituting in reference scan values and rearranging results, it can be shown [13] that the backscatter coefficient ($Sr^{-1}mm^{-1}$) is:

$$\mu_B = \frac{R_q}{2\pi(1-\cos\theta_T)} \frac{\int_{t_1}^{t_2} |V_s(t)|^2 dt}{\int_{-\infty}^{\infty} |V_q|^2 dt} \frac{4a'}{e^{-4a'd_1} - e^{-4a'd_2}}, \quad (8)$$

where θ_T is the half-angle subtended by the transducer face at the focal point, V_s is the signal obtained from the interrogated sample, integrated over the time-gate of interest, and V_q is the amplitude of the signal obtained from the ground truth reference, integrated over the full sample time.

3. Tissue Preparation

3.1. General Tissue Preparation

Porcine tissue from the oesophagus and small bowel were obtained frozen from an abattoir (Medical Meat Supplies Ltd, Oldham, UK) and the tissue samples were stored in a freezer at -4°C. These samples were assumed to be of healthy tissue as they were originally intended for human consumption. The oesophageal samples were obtained with the stomach still attached to insure presence of the gastroesophageal junction (GOJ), while the bowel samples had the mesentery and mesenteric vessels intact for perfusion purposes.

All tissue samples were initially thawed under running tap water for 20 minutes while still vacuum-packed. The thawed tissue's surface was then rinsed in tap water after removing the vacuum seal. To maintain the integrity of the tissue samples, all scanning was done in a bath of degassed phosphate buffered saline (dPBS). To obtain this, a 10 times PBS concentrate (DNase, RNase and protease free filtered through a 0.2 µm filter; pH: 7.4 +/- 0.1 contains: 11.9 mM phosphates; 137 mM NaCl; 2.7 mM

KCl, (Fisher Scientific UK Ltd, Loughborough, UK) was diluted with distilled water at a volume ratio of 1:10 and boiled for 3 minutes to degas. It was then left to cool down at room temperature overnight.

For ease and repeatability of scanning, a common tray was used which was cleaned and re-prepared for each scanning session. A 2 cm thick piece of acoustic absorber (Aptflex F28, Precision Acoustics, Dorset, UK) was placed in the bottom of the tray to prevent artefacts from stray echoes and to assist tissue pinning. To offset the tissue from the acoustic absorber base and to provide a ground truth reference for the attenuation measurements, agar was added to the containers to a height of ~4 cm. Agar-Agar granular powder, (general purpose grade, Fisher Scientific UK Ltd.) was mixed with distilled water at a mass ratio of 1:99 and boiled for 10 minutes on a hotplate whilst stirring with a magnetic stirrer. After cooling for 15 minutes at room temperature, the agar was refrigerated for 2 hours, then allowed to settle at room temperature overnight.

For each sample, a 1 - 2 mm thick layer of acoustic coupling gel was applied to the agar surface prior to pinning the tissue on top. This was used to isolate the tissue signal from the agar substrate as well as to avoid air pockets. The tissue was then immersed in dPBS to a depth sufficient to allow the ultrasound transducer to be fully submerged while maintaining the tissue in the focal zone.

3.2. Microsphere Perfusion

To prepare the bowel tissue for perfusion with fluid and the microspheres, the whole tissue was pinned down and a suitable mesenteric vessel identified and cannulated. 1 - 2 ml of red-dyed fluid were then perfused to verify the cannulation. Upon successful cannulation, a perfusion pump (Braun Perfusor, Braun, Kronberg, DE) was used to perform the main perfusion. A commercial pump was used because its over-pressure alarm prevented pressures being attained which could damage the vasculature. Once perfused, the bowel samples were opened by cutting along the upper edge of where the mesentery inserted with a scalpel, exposing the inner luminal surface of the tissue for mechanical scanning.

Control samples were infused with 50 ml of dPBS at 200 ml/hr. Microsphere samples were infused with 30 ml of dPBS at 200 ml/hr, followed by infusion of 1μm diameter fluorescent microspheres (Polysciences Inc, PA, USA) diluted in 10 ml dPBS solution at variable dilution and perfusion rates to test the impact of dilution and diffusion rate on propagation within the tissues. A final 10 ml of dPBS was then used to flush the line and ensure the same total fluid infusion between control and microsphere samples.

Surface microspheres were flushed from the samples using dPBS and the penetration of the microspheres into the sample was analysed using a fluorescent lamp (Figure 1).

3.3. Oesophageal Samples

Similar to the bowel samples, the oesophageal samples were prepared for scanning by bisecting them along the long axis using a scalpel. As the attenuation measurements require the use of a reference echo which has passed through only the tissue of interest, in this case the upper two layers, consisting of the mucosa and submucosa, two oesophageal samples were prepared using the same method as that used for the whole samples, but were then separated along the fascial plane of the tissue via blunt dissection. The mucosa - submucosal combination was separated from the remaining layers, consisting of the muscularis propria and serosa and prepared for imaging the same way as the whole tissue.

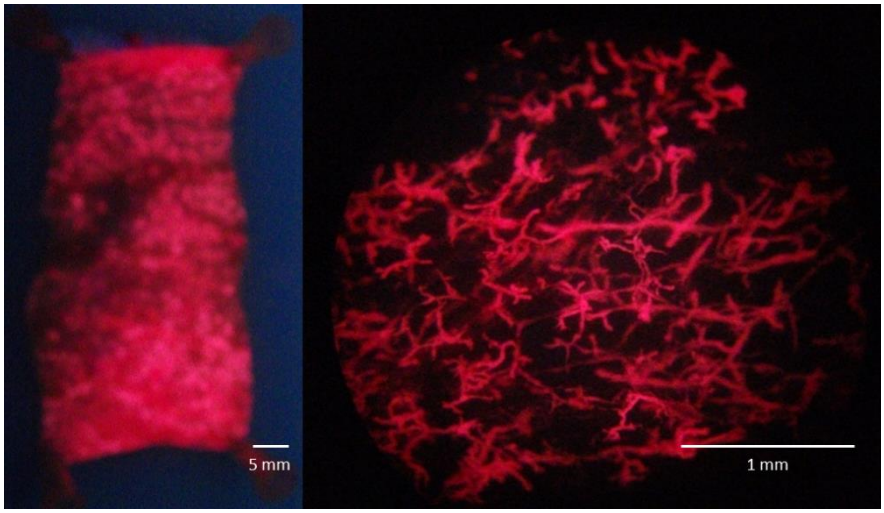

Figure 1 Microsphere-infused (1:10 volume ratio) *ex vivo* bowel tissue illuminated with a fluorescent light source. Profusion within the entire tissue sample can be seen on the left, while a 40 times magnification (right) shows that the microspheres have transited through the capillary network, but not infiltrated the interstitium or larger cellular network.

4. Scanning System

To ensure high-quality, repeatable microultrasound scans, an automated mechanical scanning system was used in all experiments to obtain the image data [14]. This system has a Labview-based (National Instruments, Austin, US) graphical user interface (GUI) used to control a pair of orthogonally-mounted linear motors supporting the scanning head of the transducer, as well as handling the triggering and data capture for the pulser/receiver unit (DPR500, JSR Ultrasonics, Pittsford, USA) and oscilloscope (MDO3014, Tektronix Inc, Beaverton, OR, USA) (Figure 2).

4.1. Scanning Software

The custom-programmed Labview GUI used to operate the microultrasound scanning system allows user control of the physical extents of each B-scan, the step size between A-scans, the time window used for capture for the RF data and any time offset. It also synchronises the triggering of the pulser/receiver unit, calibrates the digitising oscilloscope and displays and stores the data in general-use text files. The transducer used in all scanning reported here is a 48 MHz single-element transducer focused at 6 mm (AFMTH19, AFM Ltd, Birmingham, UK). The transducer was manufactured from a micromoulded PZT composite and at its focus has an axial resolution of 32 μm and a lateral resolution of 170 μm. Scans were aligned to place the centre of the tissue in the focal zone of the transducer.

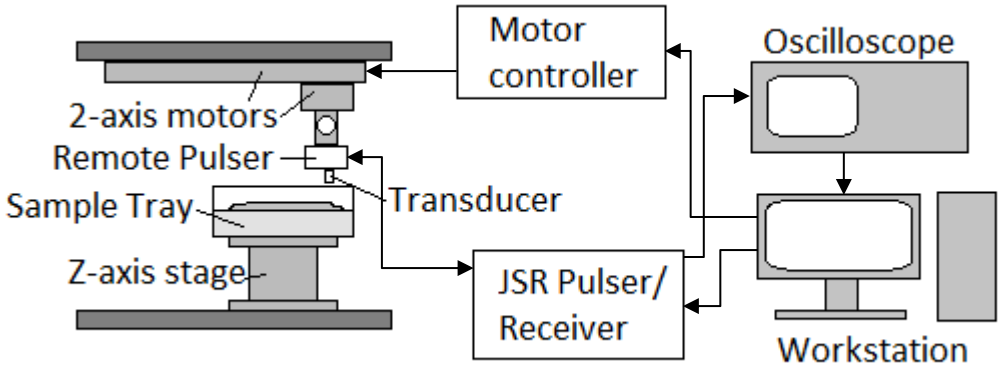

Figure 2 Mechanical scanning system used to collect the microultrasound scan data from the oesophageal and small bowel tissue samples. Communications are controlled by a custom Labview GUI on the central terminal and data is captured by the digitising oscilloscope before transfer to the terminal for display and storage.

4.2. Software Segmentation

For the acoustic property analysis techniques presented in this paper to be applicable to use *in vivo*, tissue identification and isolation must be performed digitally to ensure that the quantitative values obtained are not biased by heterogeneous tissue data. For this purpose, segmentation algorithms were developed in MATLAB (Mathworks, Natick, USA) and applied to the RF data obtained from the oesophageal tissue. The images were segmented with software masks, masking off tissue echoes below an adjustable threshold, then smoothing and hole-filling were performed to obtain a bulk zone containing the tissue of interest. Clinical judgement was used to determine the appropriate threshold for one tissue sample, then tested against the other five samples. The resulting assessment was that the mucosa/sub-mucosa had been successfully isolated from the lower layers based on a single, -26 dB threshold, referenced to the maximum echo amplitude in the image.

4.3. Quantitative Calculations

To derive the acoustic properties of the oesophageal tissue described in Section 2.2, full RF data scans were collected from the two mechanically separated tissue samples as well as a reference scan from a sample tray without a sample but with the same acoustic absorber/agar substrate and dPBS imaging medium. These data were then used to evaluate Eqn. 1 for each mechanical scan position and the mean and standard deviation were determined for each sample, as well as a weighted average for the overall sample set. A reference scan was obtained with the same agar substrate with a 0.5 mm thick quartz flat (Boston Piezo-Optics Inc., Bellingham, USA) on top to serve as a reference for the Z and BSC calculations.

5. Results

5.1. Qualitative Scans

As shown in Figure 1, while the microspheres were successfully diffused into the full breadth of the tissue sample, they were unable to extravasate the walls of the vascular system to properly simulate tissue inflammation. However, microultrasound scans performed before and after infusion, Fig. 3, show that strong μUS contrast is obtained from the microspheres and that their larger clusters can be identified and localised from qualitative imaging.

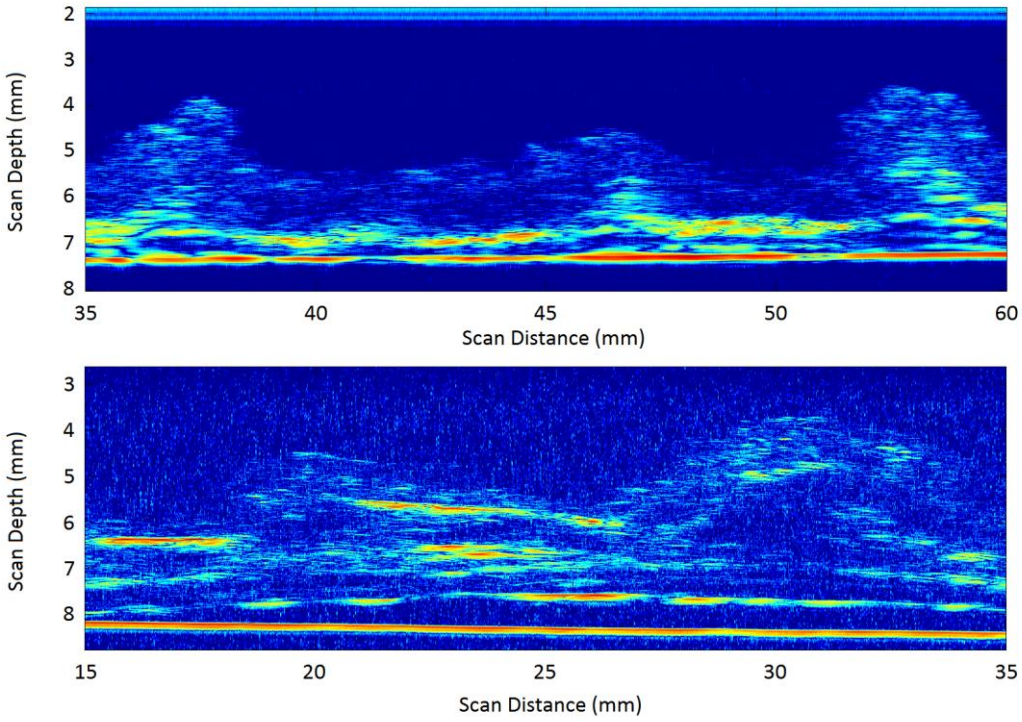

Figure 3 48 MHz μUS scans of the bowel tissue before (above) and after (below) microsphere infusion at 100 ml/hr with a 1:30 volume ratio. Microsphere concentrations can be particularly noted at the 30 mm position in the lower scan as well as by increased echo throughout the scan. Scan depth is measured with respect to the front face of the microultrasound transducer.

5.2. Quantitative Measurements

The mechanically separated oesophagus scans were used to calculate mucosal attenuation values, Fig. 4, and values of $\alpha = 1.92 \pm 0.77$ dB mm^{-1} and $\alpha = 1.78 \pm 0.66$ dB mm^{-1} were obtained as averages across each sample. $\alpha_{av} = 1.86 \pm 0.72$ dB mm^{-1}, averaged over all A-scans, was then used in the digitally separated samples.

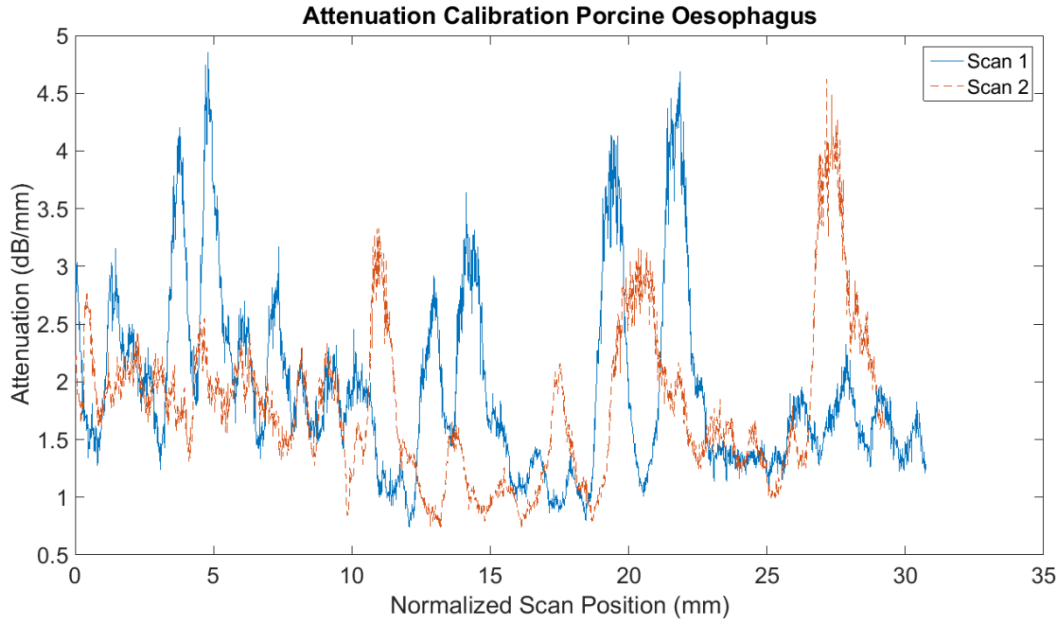

Figure 4. Attenuation as calculated from the mechanically separated oesophageal samples and agar reference substrate. Scan position is defined along the length of the tissue (oesophagus to stomach) referenced to the start of the physical scan. The two scans are for two distinct tissue samples.

The acoustic impedances and the backscatter coefficients of the six digitally segmented samples were computed and plotted for intra- and inter-sample comparison, Figs. 5 and 6. The overall mean and standard deviation values are shown in Table 1.

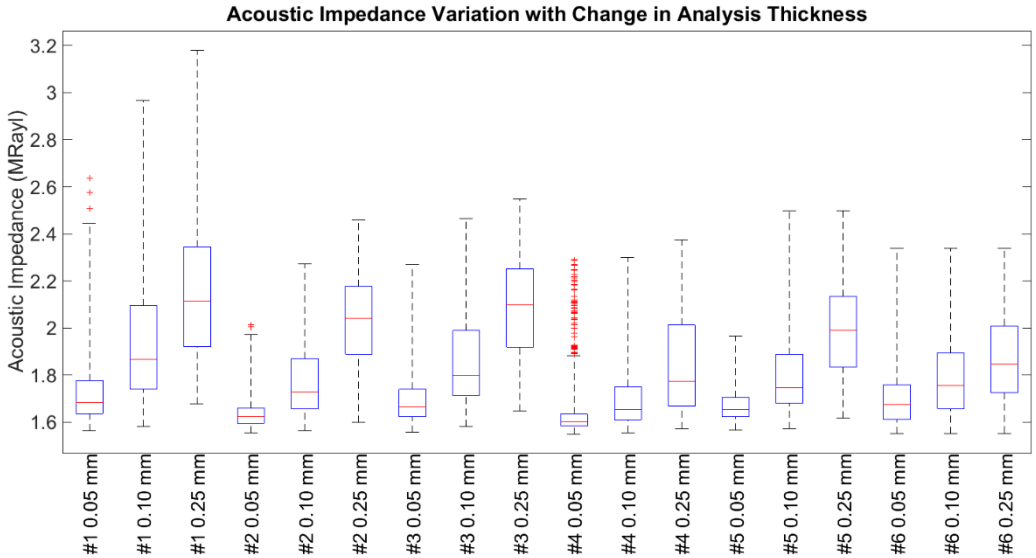

Figure 5. Acoustic Impedance of the front surface of the digitally segmented tissue samples as a function of front surface tissue thickness and sample number. Variation within each measurement is shown, with box plot depicting median, 25/75% boundary and maximum and minimum, with outliers beyond 5 times the box width marked with crosses.

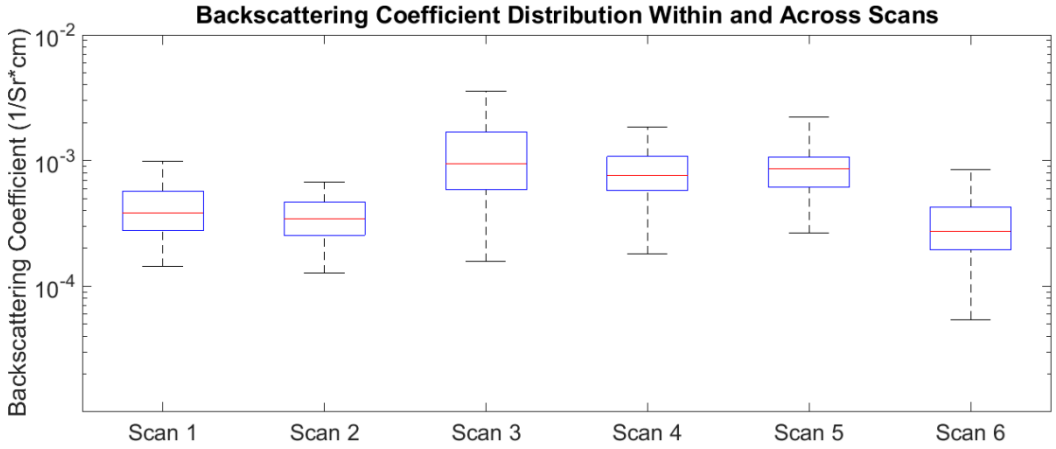

Figure 6 Backscattering coefficients for each digitally segmented tissue sample as a function of sample. Box plots indicate median, 25 and 75% extents with whiskers indicating maximum and minimum.

Table 1. Material Properties calculated for the digitally segmented porcine oesophageal samples based on the attenuation values calculated from the mechanically separated tissues.

Sample #	Z_{50} (MRayl)	Z_{100} (MRayl)	$Z2_{50}$ (MRayl)	BSC ($Sr^{-1}cm^{-1}$)
1	1.73 ± 0.15	1.95 ± 0.28	2.16 ± 0.29	$4.25 * 10^{-4} \pm 1.80 * 10^{-4}$
2	1.64 ± 0.06	1.76 ± 0.16	2.04 ± 0.18	$3.58 * 10^{-4} \pm 1.29 * 10^{-4}$
3	1.71 ± 0.12	1.86 ± 0.19	2.09 ± 0.21	$1.18 * 10^{-3} \pm 7.57 * 10^{-4}$
4	1.62 ± 0.08	1.70 ± 0.14	1.85 ± 0.21	$8.28 * 10^{-4} \pm 3.51 * 10^{-4}$
5	1.67 ± 0.07	1.80 ± 0.16	1.99 ± 0.19	$8.70 * 10^{-4} \pm 3.68 * 10^{-4}$
6	1.70 ± 0.11	1.79 ± 0.16	1.87 ± 0.17	$3.24 * 10^{-4} \pm 1.69 * 10^{-4}$

6. Discussion and Conclusions

Examination of the pre-infused microultrasound GI tissue scans show good layer differentiation. A clinician was able to identify the boundaries and thickness of the tissue layers from the B-scans, indicating that sufficient resolution was achieved for qualitative image analysis.

In the microsphere perfused scans, the microspheres could be distinguished visually, both optically and with the μUS scans, allowing verification of the scan data across the two imaging modalities. However, the lack of infiltration beyond the vascular network means that further work is required to fully mimic the behaviour of tissue inflammation. The microspheres showed good contrast in the μUS scans and the overall quality of the images validated the use of porcine tissue samples and the imaging modality for continued work in GI tissue characterisation.

The attenuation data collected from the two mechanically separated oesophageal tissue samples showed high intra-sample variation but good inter-sample agreement. This and the regularity of the variance seen in the plots suggests that high variance is normal across healthy tissue, possibly because of its convoluted surface topography. The inter-sample agreement, however, provides some confidence in the use of mean values for non-mechanically separated samples.

Overall, the acoustic impedance values calculated showed good agreement, with an increase in acoustic impedance with increasing tissue thickness. This is consistent with the known microstructure of the tissue, Fig. 7, with a highly irregular mucosal surface with deep crypts crowned with villi in the epithelium. The increase in acoustic impedance may be caused by the irregularity of the surface of the tissue columns, with more columns being included in the calculations for thicker segments. This rise

in acoustic impedance with digital segmentation thickness could provide a standard against which diseased tissue could be assessed for breakdown in the regular structures caused by cellular transformation and architectural disruption.

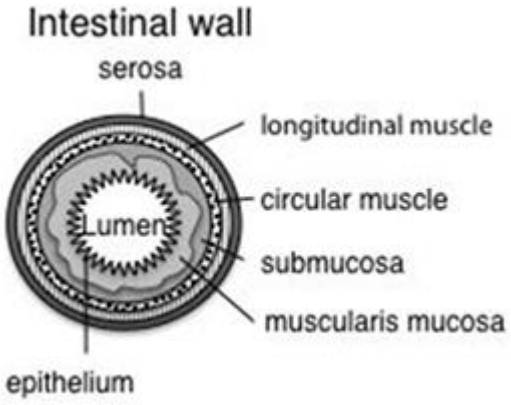

Figure 7. Anatomy of the tissue layers of the human gastrointestinal tract. All mechanical scans were performed with the epithelium facing the transducer.

The BSC values show larger variance than the acoustic impedance values, in agreement with the variability seen in the attenuation values and in the literature [15]. While studies of diseased tissue will be necessary to assess the change in mean value caused by disease progression, further steps can also be taken to reduce the large standard deviation seen in the measurements. The longitudinal plots of the attenuation values obtained from the mechanically separated samples shows relatively high variation across the tissue. This variation may contribute to the error in BSC calculations performed on the digitally segmented tissues as a mean value of attenuation was used in those measurements.

The studies presented in this work demonstrate the potential for the use of μUS imaging for GI tissue characterisation quantitatively as well as qualitatively, but challenges remain to maximise the potential. Furthermore this work illustrates the potential qualitative and quantitative μUS has in the diagnosis and management of GI disorders. The qualitative aspects of high resolution μUS would provide direct evidence of developing and evolving pathology. The quantitative facet has the potential to provide a two pronged advantage in terms of presenting data in an objective (metric'd) manner that that can be adapted into computer assisted diagnosis (CADx) thus aiding clinicians in reducing read times already associated with standard capsule endoscopy.

Acknowledgements
This work was funded by the Engineering and Physical Sciences Research Council (EPSRC) Sonopill grant (EP/K034537/1).

References

[1] U. C. Ghoshal, "Capsule Endoscopy: A New Era of Gastrointestinal Endoscopy," in *Endoscopy of GI Tract*, S. Amornyotin, Ed. InTech, 2013.
[2] G. Ciuti, A. Menciassi, and P. Dario, "Capsule Endoscopy: From Current Achievements to Open Challenges," *IEEE Rev. Biomed. Eng.*, vol. 4, pp. 59–72, 2011.
[3] B. F. Mustafa, M. Samaan, L. Langmead, and M. Khasraw, "Small bowel video capsule endoscopy: an overview," *Expert Rev. Gastroenterol. Hepatol.*, vol. 7, no. 4, pp. 323–329, May 2013.
[4] M. Rendi, "Crohn Disease Pathology: Overview, Epidemiology, Etiology," Apr. 2016.

[5] S. Ødegaard, L. B. Nesje, O. D. Lærum, and M. B. Kimmey, "High-frequency ultrasonographic imaging of the gastrointestinal wall," *Expert Rev. Med. Devices*, vol. 9, no. 3, pp. 263–273, May 2012.
[6] S. Sharma, "Micro-Ultrasound Imaging of Tissue Dysplasia," Doctoral Thesis, University of Dundee, 2015.
[7] R. K. Saha and M. C. Kolios, "Effects of cell spatial organization and size distribution on ultrasound backscattering," *IEEE Trans. Ultrason. Ferroelectr. Freq. Control*, vol. 58, no. 10, pp. 2118–2131, Oct. 2011.
[8] M. L. Oelze, J. F. Zachary, and W. D. O'Brian, Jr, "Characterization of tissue microstructure using ultrasonic backscatter: Theory and technique for optimization using a Gaussian form factor," *J. Acoust. Soc. Am.*, vol. 112, no. 3, pp. 1202–1211, Sep. 2002.
[9] E. J. Feleppa, T. Liu, A. Kalisz, M. C. Shao, N. Fleshner, V. Reuter, and W. R. Fair, "Ultrasonic spectral-parameter imaging of the prostate," *Int. J. Imaging Syst. Technol.*, vol. 8, no. 1, pp. 11–25, Jan. 1997.
[10] J. Jankowski, H. Barr, K. Wang, and B. Delaney, "Diagnosis and management of Barrett's oesophagus," *BMJ*, vol. 341, p. c4551, 2010.
[11] L. Schantz, K. Laber-Laird, S. Bingel, and M. Swindle, *Essentials of Experimental Surgery: Gastroenterology*. CRC Press, 1996.
[12] H. W. Siesler, "12.3.1 Influence of Fixation on Acoustic Parameters of Cells and Tissues," in *Biomedical Imaging: Principles and Applications*, John Wiley & Sons, Inc., 2012.
[13] F. S. Foster, M. Strban, and G. Austin, "The Ultrasound Macroscope: Initial Studies of Breast Tissue," *Ultrason. Imaging*, vol. 6, pp. 243–261, 1984.
[14] T. Anbarasan, C. Demore, H. Lay, M. Sunoqrot, R. Poltarjonoks, S. Cochran, and B. Cox, "Development of small bowel tissue phantom for microultrasound (uUS) investigation," in *Biosensor Technologies*, A. Rasooly and B. Pickril, Eds. Springer, 2016.
[15] C. M. Moran, N. L. Bush, and J. C. Bamber, "Ultrasonic Propagation Properties of Excised Human Skin," *Ultrasound Med. Biol.*, vol. 21, no. 9, pp. 1177–1190, 1995.